Mechanical and phase transformation behaviour of biomedical Co-Cr-Mo alloy fabricated by direct metal laser sintering

M. Béreš[a], C.C. Silva[b], P.W.C. Sarvezuk[c], L. Wu[d], L.H.M. Antunes[e,*], A.L. Jardini[a], A.L.M. Feitosa[b], J. Žilková[f], H.F.G. de Abreu[b], R.M. Filho[a]

[a] National Institute of Biofabrication, Faculty of Chemical Engineering, State University of Campinas, Av. Albert Einstein 500, 13083-852 Campinas, SP, Brazil
[b] Department of Metallurgical and Materials Engineering, Federal University of Ceará, Campus do Pici, Bloco 729, 60440-554 Fortaleza, CE, Brazil
[c] Department of Physics, State University of Maringá, Av. Colombo 5790, CEP 87020-900 Maringá, PR, Brazil
[d] Brazilian Nanotechnology National Laboratory – LNNano, CNPEM, R. Giuseppe Máximo Scolfaro 10000, 13083-970 Campinas, SP, Brazil
[e] Faculty of Mechanical Engineering, State University of Campinas, Av. Albert Einstein 500, 13083-852 Campinas, SP, Brazil
[f] Department of Electrical Engineering and Mechatronics, Technical University of Košice, Letná 9, 042 00 Košice, Slovak Republic

A B S T R A C T

Biomedical cobalt-chromium-molybdenum (Co-Cr-Mo) alloys have been used in the cast or wrought form as prosthetic implant materials for more than five decades. Recently, additive manufacturing techniques are employed to produce parts directly from metal precursor powder with a composition suitable for biomedical applications. In the work present, we examine both mechanical behaviour and $\gamma \rightarrow \varepsilon$ phase transformation in the heat treated Co-Cr-Mo alloy fabricated via additive manufacturing route. Results suggest, that selection of appropriate heat treatment and control of martensitic transformation can significantly influence mechanical properties. The studied Co-Cr-Mo alloy can be considered as a potential material for biomedical applications.

1. Introduction

The use of metal-on-metal bearings in total hip arthroplasties allows deployment of large diameter femoral head (> 32 mm) components [1,2]. Such design offers greater range of motion, reduces risk of component-to-component impingement [3,4], while providing reduced articular wear. For several decades, biomedical cobalt-chrome-molybdenum (Co-Cr-Mo) alloys are employed for this application due to their favourable properties including high strength combined with excellent corrosion and wear resistance [5–7]. The wear resistance of these alloys is usually attributed to increased strain hardening and formation of carbide or nitride precipitates [8,9]. Recently it was reported, that the wear resistance and strength can be altered through control of martensitic transformation [10,11]. Cobalt-base alloys undergoes an allotropic transformation at around 970 °C [12] from a high temperature face-centered cubic (fcc) γ phase to a room temperature hexagonal close-packed (hcp) ε phase. The hcp phase can be obtained by slow cooling; through an isothermal transformation – usually maintaining the sample at around 800 °C [13], or through strain. The

fcc phase can be easily stabilised at low temperatures through fast cooling, so is common to have a metastable γ fcc phase at room temperature which can transform to a thermodynamically stable ε hcp martensitic phase [14] by strain induced martensitic transformation mechanism (SIMT). In this alloy system, the SIMT occurs if the atomic stacking sequence of ABC-type in the γ phase is altered to the hexagonal ABA-type by introducing of stacking fault on every second $\{111\}_\gamma$ plane [15]. This transition is caused by $\{111\} < 11\text{-}2 >$ type shear of fcc lattice via motion of $a/6 < 11\text{-}2 >$ Shockley partial dislocations and strongly depends on stacking fault energy (SFE) [10]. With the decreasing SFE, the width of stacking faults between Shockley partial dislocations increases. Consequently, wide stacking faults are formed in alloys with a low SFE. Remy and Pineau [16] reported that in Co-base alloys the SIMT occurred with SFE below 15 mJ m^{-2}. Deformation twinning and dislocation slip is commonly observed at higher values of SFE [17].

Co-Cr-Mo alloys are conventionally produced via casting followed by thermomechanical treatment in addition to powder metallurgy route [8]. These production processes may suffer some limitations because

---

Table 1
Chemical composition of studied laser sintered sample (wt%).

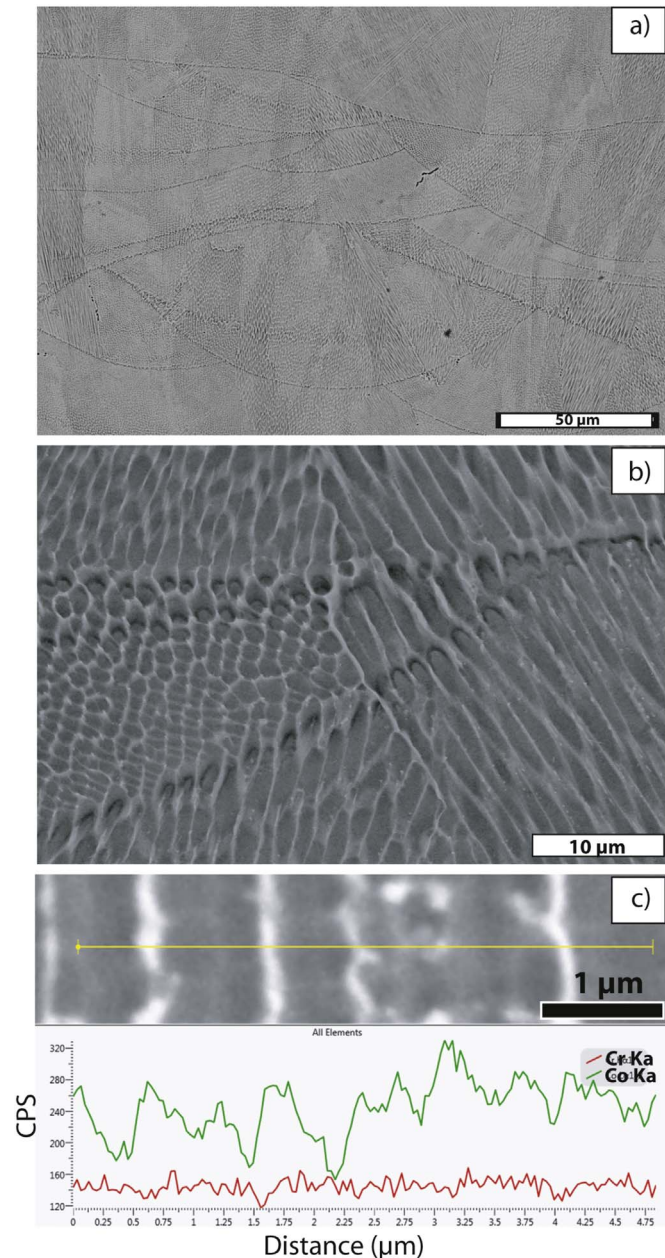| Co	Cr	Mo	Si	Mn	Fe	Ni
63.45	28.14	6.91	0.65	0.72	0.08	0.05

Fig. 1. a) and b) SEM BSE micrograph of the laser sintered sample showing cellular dendritic microstructure. Energy dispersive spectroscopy (EDS) scan across dendrites revealing presence of microsegregation in interdendritic regions, c).

components with complex shapes and satisfactorily mechanical properties are difficult to achieve. Recently, additive manufacturing techniques such as electron beam melting or direct metal laser sintering (DMLS) [18–22], being employed to fabricate near-net-shape

components for both aerospace [23] and biomedical applications [24–30] directly from metal powder. The DMLS technique is a computer assisted process where laser fuses metal powder in layer-by-layer manner. Depends on local solidification conditions during the additive manufacturing process, columnar and/or equiaxed grains can develop throughout the volume of the build [23]. The formation of columnar grains can lead to anisotropic materials properties [31–34]. In case of fcc alloys, the solidification texture depends on the local heat flow directions and competitive grain growth in one of the six < 100 > preferred growth directions [35]. It is obvious, that control of microstructure, texture and phase transformation is crucial when designing well-functioning implant alloy. Although both texture and the SIMT have been systematically studied in conventionally produced Co base alloys [36], the γ→ε phase transformation of material fabricated by additive manufacturing techniques has not yet been examined thoroughly.

In the work present, we analyse γ→ε phase transformation before and after straining of the heat treated Co-Cr-Mo samples that were produced via DMLS route employing both electron backscattered diffraction and X-Ray diffraction techniques. In addition, mechanical behaviour of the heat treated material was examined.

2. Experimental

2.1. Fabrication of samples and heat treatment

Samples for microstructural characterisation and tensile tests were fabricated using EOSINT 280 DMLS machine (EOS GmbH, Germany) with MP1 Co-Cr-Mo metallic powder feedstock [37] being supplied by EOS GmbH, Germany. Using the MP1 prescribed parameter set, powder was sintered layer by layer with Yb-fibre laser with nominal power of 200 W and laser spot diameter of 100 μm. The building platform was heated to 80 °C and the oxygen content in the process chamber was maintained below 0.1%. A continuous laser beam-scanning mode was employed with a meander scan strategy (67° rotation for each layer). The laser sintered samples were solution treated at 1150 °C for 1 h followed by water quenching. Then, one batch of the samples was additionally isothermally heat treated at 800 °C for 4 h and quenched in water. The specimens were prepared and examined parallel to the build direction plane.

2.2. Mechanical testing

Tensile tests samples with cross section 6 × 2 mm^2 were prepared following ASTM E8 standard. Tensile tests were conducted on an MTS 810 - FlexTest 40 tension/compression servohydraulic testing machine fitted with 100 kN load cell. The tests were performed with crosshead displacement rate of 2 mm/min at room temperature. The average strain over a 25 mm gauge length was recorded with a MTS 632.24C-50 extensometer. Sections in the proximity to the fractured surface were used for electron backscattered diffraction (EBSD) analysis.

2.3. Microstructural characterisation

Samples for both microstructural characterisation and diffraction studies were polished electrolytically using solution of 5 vol% concentrated perchloric acid in an acetic acid base electrolyte under applied voltage of 21 V at temperature of 15 °C. The electropolished samples were examined by backscattered electron imaging. In addition, microstructural characterisation was carried out on miniature tensile test specimens with cross section 1 × 1 mm^2. On these samples, EBSD

maps were acquired from the identical region at 0% and 2% plastic deformation. To ensure that maps are collected from the same region, micro hardness indents as fiducial mark points were made at the sample's gauge centre. In addition, EBSD maps were obtained from regions in the vicinity of the fractured surface of the tensile tests specimens parallel to the load axis. Samples for the EBSD analysis were prepared by electrolytical polishing and further polishing on Buehler VibroMet™ 2 Vibratory Polisher using colloidal silica for duration of several hours. Microstructural characterisation was carried out on a FEI Quanta 450 and FEI Quanta 650 scanning electron microscopes (SEM), both fitted with HKL Nordlys orientation imaging system (Oxford Instruments, Oxford, UK). EBSD maps were acquired using AZtecHKL software. The HKL Channel 5 software package (Oxford Instruments, Oxford, UK) was used to process the EBSD data.

2.4. X-ray diffraction (XRD)

XRD measurements in the angular range 2θ = 35–85° were carried out using a Philips® X′Pert Pro diffractometer equipped with Co Kα radiation source applying voltage and current of 40 kV and 45 mA, respectively. The obtained diffraction patterns were compared with data from the ICSD database in order to identify phases present.

3. Results and discussion

The chemical composition of the CoCrMo of laser sintered sample obtained by x-ray fluorescence is detailed in Table 1.

Fig. 1a) and b) shows SEM backscattered electron micrographs after electropolishing of the laser sintered sample. The microstructure consists of fine cellular dendrites in addition to laser tracks. The interdendritic spacing is approximately 1 μm. The cellular dendrites are not confined by the weld pool and in general intersect the weld pool boundaries. A presence of cellular dendrites is caused by fast cooling rate during solidification of the molten metal during the build process and is consistent with observations in refs. [32,35]. Such microstructural features can lead to anisotropic properties [32] which is of concern for materials to be used in biomedical applications. Fig. 1c) shows energy dispersive spectroscopy (EDS) scan across dendrites revealing presence of microsegregation, in particular Co in interdendritic regions which can enhance crack propensity.

In order to eliminate the dendritic microstructure and microsegregation of the laser sintered sample, a solution annealing treatment was carried out. This consisted of heating of samples to 1150 °C followed by water quenching. Some solution treated samples were subjected to isothermal heat treatment at 800 °C for 4 h and quenched in water. This treatment aimed to increase both tensile strength and yield stress by diffusionaly formed hcp ε phase finely distributed in the fcc γ matrix.

Fig. 2 shows XRD profiles of solution treated sample (black line) where fcc γ phase (ICSD card # 52934) was identified. In the specimen subjected to solution annealing + isothermal treatment at 800 °C for 4 h (grey line), in addition to the fcc γ phase a hcp ε phase (ICSD card # 53806) was detected. The formation of isothermal ε martensite in this temperature range is in good agreement with results reported in refs. [38,39] for forged alloy. It is to be noted that from the diffraction peaks it was not possible to distinguish between isothermal and athermal (not shown here) martensitic phase. This was possible however by means of EBSD analysis which is presented in sections below.

Fig. 3 shows engineering stress-strain curves of solution treated (ST) specimen in addition to sample subjected to ST + isothermal treatment at 800 °C for 4 h. The measured yield stress of the ST specimen was below that of ST + isothermaly treated sample (612 vs. 765 MPa).
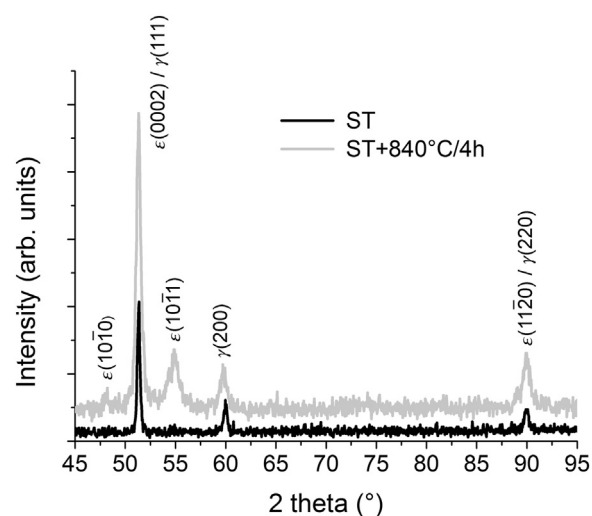

Fig. 2. XRD patterns obtain in both solution treated (ST) specimen and sample subjected to ST + isothermal treatment at 800 °C for 4 h.
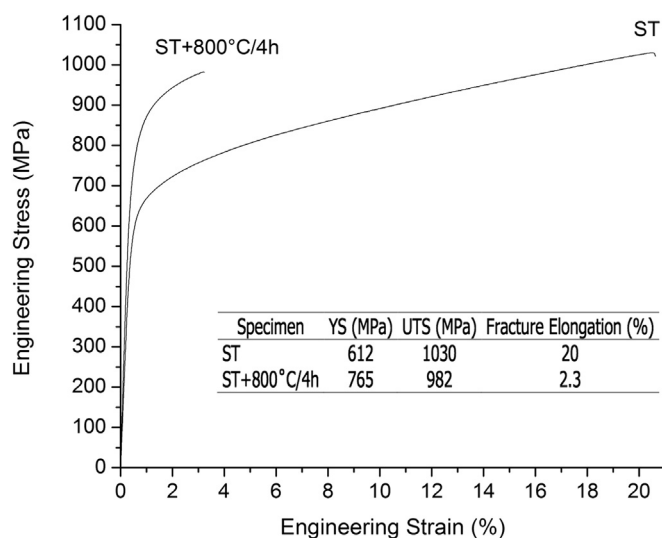

Fig. 3. Engineering stress-strain curves of solution treated (ST) specimen and sample subjected to ST + isothermal treatment at 800 °C for 4 h. In the insert table, mechanical properties obtained are shown.

Saldívar Garcia et al. (1999) and Kurosu et al. (2010) have described a 50% increase in hardness and yield strength of a sample transforming from a total cubic structure to a total hexagonal one [12,40]. The higher yield stress of the isothermally treated specimen can be attributed to the formation of finely distributed hcp phase in the fcc {111} planes which can restrict dislocation slip in the fcc lattice [39]. The formation of the hcp phase during isothermal heat treatment, Fig. 2, may also be the reason for both the lower ductility and inferior ultimate tensile strength. Isothermally formed hcp phase is known to decrease ductility due to the localised stress concentration at interfaces [41]. Indeed, in the ST + isothermally treated specimen a premature failure with small plastic deformation ~2.3% occurred and this sample fractured prior to the onset of plastic instability. Since less work hardening could take place in this condition, the achieved ultimate tensile strength was 982 MPa. Evaluating the initial microstructure of the ST specimen prior to deformation, it essentially consists of fcc phase, Fig. 2. As noted
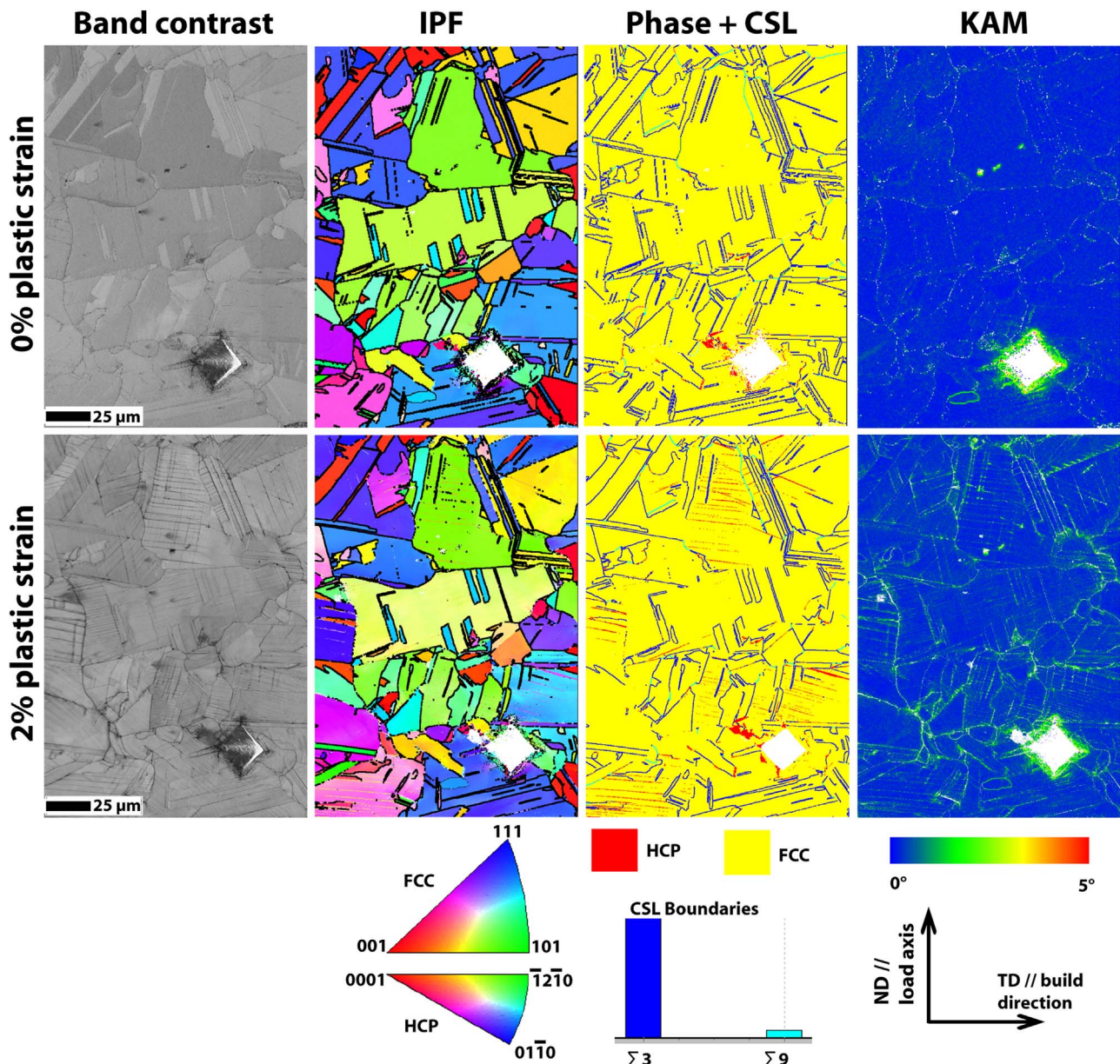
Fig. 4. EBSD orientation maps in longitudinal section view of specimen subjected to solution treatment and isothermal dwell at 800 °C for 4 h at 0% deformation and corresponding map after 2% plastic strain showing evidence of strain-induced transformation. The colours in the inverse pole figure (IPF) map indicate the orientation of grains with respect to the crystal reference frame according to the IPF triangle shown below the map. In these maps, thick black lines represent high angle grain boundaries (misorientation greater than 10 degrees), whereas thin black lines represent low angle grain boundaries (misorientation less than 2 degrees). In the phase map, the fcc phase is coloured in yellow, the hcp phase in red and annealing twins are highlighted in dark blue. The Kernel Average Misorientation (KAM) map shows average misorientation angle of a given point and the average orientation of the neighbour's grains. The scale bar of 25 μm is the same for all maps. (For interpretation of the references to color in this figure legend, the reader is referred to the web version of this article.)

previously, analysis of engineering stress-strain curve for this condition revealed that the plastic deformation initiate at 612 MPa. However, during further straining, the sample experiences a significant strengthening in the plastic deformation regime reaching ultimate tensile strength of 1030 MPa which is higher than in the other sample. Several factors may be associated with this increment of strength. The formation of deformation twins and phase transformation can be responsible for accommodation of stresses in the early stage of deformation [42]. Twin boundaries serves as barriers for dislocation slip

which enhances work hardening [43,44]. Deformation twin boundaries play an important role in increase of strength of fcc alloys, acting as barriers for dislocation slip which enhances work hardening [12,45,46]. Moreover, the ST specimen shows fracture elongation of 20% which is more than 8 times higher in comparison to the other sample. The greater ductility in the ST specimen may be associated with more slip systems available in fcc matrix which facilitates dislocation glide in addition to twin induced plasticity.

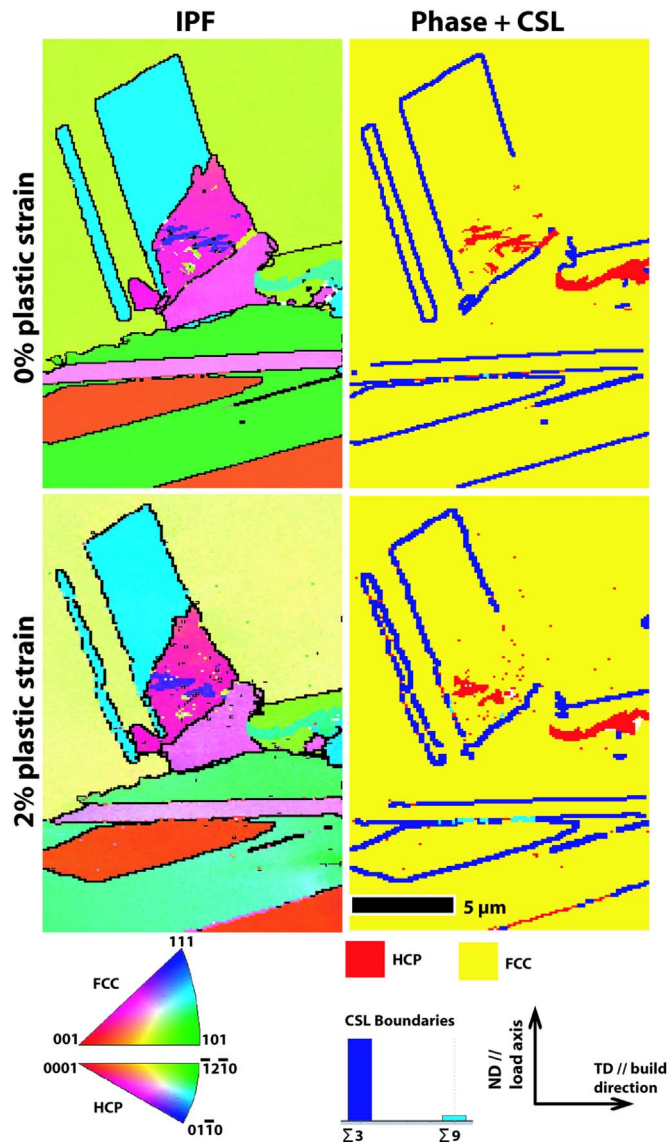SEM EBSD micrograph of alloy after solution heat treatment and

Fig. 5. EBSD maps from depicted region in Fig. 4 at 0% deformation and corresponding map after 2% plastic strain. Left hand side inverse pole figure (IPF) map, right hand side a composition of phase map with coincidence-site lattice (CSL) map revealing formation of hcp ε phase at coherent Σ3 twins – highlighted in dark blue. The scale bar of 5 μm is the same for all maps. (For interpretation of the references to color in this figure legend, the reader is referred to the web version of this article.)

coherent annealing twins are formed during solution annealing and were reported previously in a conventional alloy and similar heat treatment condition [15]. The Kernel Average Misorientation (KAM) map shows homogenous distribution with grain to grain misorientation lower than 1°. The microstructural features observed are in good agreement with those reported previously [48] for wrought Co-Cr-Mo alloy.

EBSD analysis was carried out in the same region after 2% plastic deformation and the results are presented in Fig. 4, bottom part. One can observe formation of hcp phase formed by SIMT mechanism, coloured in red in the phase map. The hcp phase is formed in both interior of grains and at annealing twin boundaries. Thus, even in small quantities, the hcp phases formed during plastic deformation will contribute to an increase of tensile strength by pinning dislocation slip. The KAM map shows an increase in grain to grain misorientation up to 4° at the interfaces fcc/hcp phases in the strained sample. Although the hcp phase formed by SIMT mechanism contributes to an increase of both the strength and wear resistance, it can be detrimental to the cold deformation [15]. This is due fact that the initiation and propagation of cracks occur at and/or along hcp phase [15].

Fig. 5 shows magnified EBSD maps from depicted region in Fig. 4 at 0% deformation and corresponding map after 2% plastic strain. In the phase map at 0% deformation it is possible to observe hcp ε phase that was formed through diffusional mechanism. In the phase map acquired after 2% plastic strain, one can observe that the hcp ε phase is generated at the annealing twin boundaries through SIMT mechanism.

Fig. 6 shows EBSD maps collected in distance of approximately between 0 and 5 μm from the fractured plane of the tensile test specimen that was subjected to solution heat treatment and isothermal dwell at 800 °C for 4 h. In the vicinity of the fracture one can expect largest strain. Therefore, a large (~44 vol%) volumetric fraction of the hcp ε phase formed by SIMT mechanism was identified in Fig. 6c. One can observe that almost entire fracture surface is decorated with the ε hcp phase, indicating that the initiation and propagation of cracks occur at the hcp phase. In addition, a high grain-to-grain misorientation is present as revealed in Kernel average misorientation map, Fig. 6d, causing development of high intergranular strain. This can contribute to a premature fracture. These findings are in good agreement with those reported previously by conventionally produced Co-Cr-Mo alloy [10,15]. When considering mechanical properties and phase transformation behaviour, the laser sintered Co-Cr-Mo alloy behaves in a similar manner as a conventionally produced cast and/or forged alloy and can be considered as a potential material for biomedical applications. Prior to this however, a comprehensive materials characterisation including fatigue, wear and corrosion resistance tests in addition to both in vivo and in vitro studies are required.

4. Conclusions

Mechanical properties and strain induced martensitic transformation were analysed in biomedical Co-Cr-Mo alloy produced by direct metal laser sintering additive manufacturing method.

- In the laser sintered material a dendritic microstructure with microsegregation is formed which can be eliminated by appropriate heat treatment.
- A good combination of mechanical properties was achieved in the solution treated material.
- The γ→ε martensitic transformation significantly influences mechanical properties.
- Crack initiation and propagation occurs preferentially at the ε martensite.
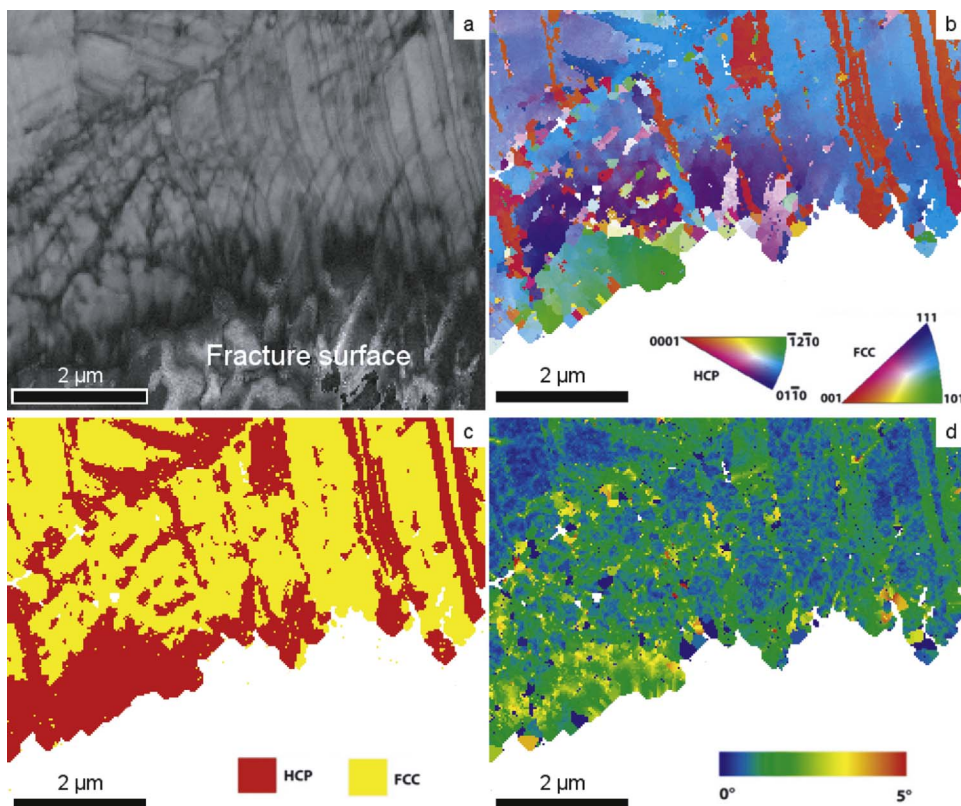
isothermal dwell at 800 °C for 4 h is shown in Fig. 4, upper part. Grains with annealing twins are visible in band contrast map at 0% plastic deformation. The average grain size determined by intercept method is 45 μm. The solution treatment successfully eliminated dendritic microstructure. Precipitates such as carbides (i.e. type $M_{23}C_6$ and M_6C) that are commonly reported in cast Co-Cr-Mo alloys [47] could not be identified from this map. The inverse pole figure (IPF) map does not show preferential orientation of grains. The phase map revealed fcc matrix (yellow) with traces of granular grains of hcp crystal structure (red). It could be confirmed that the hcp ε grains are formed by diffusion (isothermal martensite) during isothermal treatment at 800 °C, except of that induced by deformation (athermal martensite) in the vicinity of the indentation point. The coincidence site lattice (CSL) map revealed presence of coherent Σ3 twins – highlighted in dark blue. The

Fig. 6. EBSD maps collected in distance of approximately 5 μm from the fractured plane of the tensile test specimen subjected to solution treatment and isothermal dwell at 800 °C for 4 h. a) band contrast map, b) IPF map, c) phase map, d) Kernel average misorientation map.

Acknowledgments

Authors are grateful for the assistance L.F. Bernardes with fabrication of the samples. Experimental support of J.L. Lisboa (FEM Unicamp), Dr. F.E. Montoro and Dr. A.L. Gobbi (projects SEM 21795 and LMF 20869) at Brazilian Nanotechnology National Laboratory-LNNano in addition to help provided by members of Materials Group at Brazilian Synchrotron Light Laboratory-LNLS is acknowledged. This work was financially supported by CAPES and São Paulo Research Foundation FAPESP (grant number 2016/09350-2). Microstructural characterisation was performed at Analytical Centre – UFC/CT-INFRA/MCTI-SISNANO/Pró-Equipamentos CAPES and LNNano.

References

[1] K. Yamanaka, M. Mori, Y. Koizumi, A. Chiba, Local strain evolution due to athermal γ→ε martensitic transformation in biomedical Co Cr Mo alloys, J. Mech. Behav. Biomed. Mater. 32 (2014) 52–61, http://dx.doi.org/10.1016/j.jmbbm.2013.12.019.
[2] E.J. Silverman, B. Ashley, N.P. Sheth, Metal-on-metal total hip arthroplasty: is there still a role in 2016? Curr. Rev. Musculoskelet. Med. 9 (2016) 93–96, http://dx.doi.org/10.1007/s12178-016-9323-1.
[3] J.M. Cuckler, K.D. Moore, A.V. Lombardi, E. McPherson, R. Emerson, Large versus small femoral heads in metal-on-metal total hip arthroplasty, J. Arthroplast. 19 (2004) 41–44, http://dx.doi.org/10.1016/j.arth.2004.09.006.
[4] B.R. Burroughs, B. Hallstrom, G.J. Golladay, D. Hoeffel, W.H. Harris, Range of motion and stability in total hip arthroplasty with 28-, 32-, 38-, and 44-mm femoral head sizes, J. Arthroplast. 20 (2005) 11–19, http://dx.doi.org/10.1016/j.arth.2004.07.008.
[5] J.H. Dumbleton, M.T. Manley, Metal-on-metal total hip replacement, J. Arthroplast. 20 (2005) 174–188, http://dx.doi.org/10.1016/j.arth.2004.08.011.
[6] Y. Koizumi, Y. Chen, Y. Li, K. Yamanaka, A. Chiba, S.-I. Tanaka, Y. Hagiwara, Uneven damage on head and liner contact surfaces of a retrieved Co–Cr-based metal-on-metal hip joint bearing: an important reason for the high failure rate, Mater. Sci. Eng. C 62 (2016) 532–543, http://dx.doi.org/10.1016/j.msec.2016.01.006.
[7] S. Kurosu, H. Matsumoto, A. Chiba, C. Landron, D. Fabregue, E. Maire, The damage process in a biomedical Co–29Cr–6Mo–0.14N alloy analyzed by X-ray tomography and electron backscattered diffraction, Scr. Mater. 64 (2011) 367–370, http://dx.doi.org/10.1016/j.scriptamat.2010.07.032.
[8] K.C. Antony, Wear-resistant cobalt-base alloys, JOM 35 (1983) 52–60, http://dx.

doi.org/10.1007/BF03338205.
[9] K.R. John St., L.D. Zardiackas, R.A. Poggie, Wear evaluation of cobalt-chromium alloy for use in a metal-on-metal hip prosthesis, J. Biomed. Mater. Res. 68B (2004) 1–14, http://dx.doi.org/10.1002/jbm.b.10053.
[10] B.-S. Lee, Y. Koizumi, H. Matsumoto, A. Chiba, Collective behavior of strain-induced martensitic transformation (SIMT) in biomedical Co–Cr–Mo–N alloy polycrystal: an ex-situ electron backscattering diffraction study, Mater. Sci. Eng. A 611 (2014) 263–273, http://dx.doi.org/10.1016/j.msea.2014.05.071.
[11] R.T. Smith, T. Lolla, D. Gandy, L. Wu, G. Faria, A.J. Ramirez, S.S. Babu, P.M. Anderson, In situ X-ray diffraction analysis of strain-induced transformations in Fe- and Co-base hardfacing alloys, Scr. Mater. 98 (2015) 60–63, http://dx.doi.org/10.1016/j.scriptamat.2014.11.003.
[12] A.D.J. Saldívar García, A.M. Medrano, A.S. Rodríguez, Formation of hcp martensite during the isothermal aging of an fcc Co-27Cr-5Mo-0.05C orthopedic implant alloy, Metall. Mater. Trans. A 30 (1999) 1177–1184, http://dx.doi.org/10.1007/s11661-999-0267-6.
[13] S. Cai, M.R. Daymond, Y. Ren, Stress induced martensite transformation in Co–28Cr–6Mo alloy during room temperature deformation, Mater. Sci. Eng. A 580 (2013) 209–216, http://dx.doi.org/10.1016/j.msea.2013.05.050.
[14] G.B. Olson, M. Cohen, A mechanism for the strain-induced nucleation of martensitic transformations, J. Less Common Met. 28 (1972) 107–118, http://dx.doi.org/10.1016/0022-5088(72)90173-7.
[15] Y. Koizumi, S. Suzuki, K. Yamanaka, B.-S. Lee, K. Sato, Y. Li, S. Kurosu, H. Matsumoto, A. Chiba, Strain-induced martensitic transformation near twin boundaries in a biomedical Co–Cr–Mo alloy with negative stacking fault energy, Acta Mater. 61 (2013) 1648–1661, http://dx.doi.org/10.1016/j.actamat.2012.11.041.
[16] L. Remy, Kinetics of strain-induced fcc→hcp martensitic transformation, Metall. Trans. A 8 (1977) 253–258, http://dx.doi.org/10.1007/BF02661637.
[17] G.B. Olson, M. Cohen, A general mechanism of martensitic nucleation: part I. General concepts and the FCC → HCP, Transform., Metall. Trans. A 7 (1976) 1897–1904, http://dx.doi.org/10.1007/BF02659822.
[18] T.M. Mower, M.J. Long, Mechanical behavior of additive manufactured, powder-bed laser-fused materials, Mater. Sci. Eng. A 651 (2016) 198–213, http://dx.doi.org/10.1016/j.msea.2015.10.068.
[19] A. Simchi, Direct laser sintering of metal powders: mechanism, kinetics and microstructural features, Mater. Sci. Eng. A 428 (2006) 148–158, http://dx.doi.org/10.1016/j.msea.2006.04.117.
[20] S. Sarkar, C. Siva Kumar, A. Kumar Nath, Effect of mean stresses on mode of failures and fatigue life of selective laser melted stainless steel, Mater. Sci. Eng. A 700 (2017) 92–106, http://dx.doi.org/10.1016/j.msea.2017.05.118.
[21] B. Clausen, D.W. Brown, J.S. Carpenter, K.D. Clarke, A.J. Clarke, S.C. Vogel, J.D. Bernardin, D. Spernjak, J.M. Thompson, Deformation behavior of additively manufactured GP1 stainless steel, Mater. Sci. Eng. A 696 (2017) 331–340, http://dx.doi.org/10.1016/j.msea.2017.04.081.

[22] H.D. Carlton, A. Haboub, G.F. Gallegos, D.Y. Parkinson, A.A. MacDowell, Damage evolution and failure mechanisms in additively manufactured stainless steel, Mater. Sci. Eng. A 651 (2016) 406–414, http://dx.doi.org/10.1016/j.msea.2015.10.073.

[23] S.S. Babu, L. Love, R. Dehoff, W. Peter, T.R. Watkins, S. Pannala, Additive manufacturing of materials: opportunities and challenges, MRS Bull. 40 (2015) 1154–1161, http://dx.doi.org/10.1557/mrs.2015.234.

[24] L.E. Murr, S.M. Gaytan, E. Martinez, F. Medina, R.B. Wicker, Next generation orthopaedic implants by additive manufacturing using electron beam melting, Int. J. Biomater. 2012 (2012) 1–14, http://dx.doi.org/10.1155/2012/245727.

[25] J.J. de Damborenea, M.A. Larosa, M.A. Arenas, J.M. Hernández-López, A.L. Jardini, M.C.F. Ierardi, C.A.C. Zavaglia, R.M. Filho, A. Conde, Functionalization of Ti6Al4V scaffolds produced by direct metal laser for biomedical applications, Mater. Des. 83 (2015) 6–13, http://dx.doi.org/10.1016/j.matdes.2015.05.078.

[26] Y. Koizumi, A. Okazaki, A. Chiba, T. Kato, A. Takezawa, Cellular lattices of biomedical Co-Cr-Mo-alloy fabricated by electron beam melting with the aid of shape optimization, Addit. Manuf. 12 (2016) 305–313, http://dx.doi.org/10.1016/j.addma.2016.06.001.

[27] S.M. Gaytan, L.E. Murr, E. Martinez, J.L. Martinez, B.I. Machado, D.A. Ramirez, F. Medina, S. Collins, R.B. Wicker, Comparison of microstructures and mechanical properties for solid and mesh cobalt-base alloy prototypes fabricated by electron beam melting, Metall. Mater. Trans. A. 41 (2010) 3216–3227, http://dx.doi.org/10.1007/s11661-010-0388-y.

[28] E. Sallica-Leva, A.L. Jardini, J.B. Fogagnolo, Microstructure and mechanical behavior of porous Ti–6Al–4V parts obtained by selective laser melting, J. Mech. Behav. Biomed. Mater. 26 (2013) 98–108, http://dx.doi.org/10.1016/j.jmbbm.2013.05.011.

[29] E. Marin, S. Fusi, M. Pressacco, L. Paussa, L. Fedrizzi, Characterization of cellular solids in Ti6Al4V for orthopaedic implant applications: trabecular titanium, J. Mech. Behav. Biomed. Mater. 3 (2010) 373–381, http://dx.doi.org/10.1016/j.jmbbm.2010.02.001.

[30] J. Parthasarathy, B. Starly, S. Raman, A. Christensen, Mechanical evaluation of porous titanium (Ti6Al4V) structures with electron beam melting (EBM), J. Mech. Behav. Biomed. Mater. 3 (2010) 249–259, http://dx.doi.org/10.1016/j.jmbbm.2009.10.006.

[31] J.J. Lewandowski, M. Seifi, Metal additive manufacturing: a review of mechanical properties, Annu. Rev. Mater. Res. 46 (2016) 151–186, http://dx.doi.org/10.1146/annurev-matsci-070115-032024.

[32] A. Takaichi, Suyalatu, T. Nakamoto, N. Joko, N. Nomura, Y. Tsutsumi, S. Migita, H. Doi, S. Kurosu, A. Chiba, N. Wakabayashi, Y. Igarashi, T. Hanawa, Microstructures and mechanical properties of Co-29Cr-6Mo alloy fabricated by selective laser melting process for dental applications, J. Mech. Behav. Biomed. Mater. 21 (2013) 67–76, http://dx.doi.org/10.1016/j.jmbbm.2013.01.021.

[33] E.E. de Obaldia, C. Jeong, L.K. Grunenfelder, D. Kisailus, P. Zavattieri, Analysis of the mechanical response of biomimetic materials with highly oriented microstructures through 3D printing, mechanical testing and modeling, J. Mech. Behav.

Biomed. Mater. 48 (2015) 70–85, http://dx.doi.org/10.1016/j.jmbbm.2015.03.026.

[34] M. Simonelli, Y.Y. Tse, C. Tuck, Effect of the build orientation on the mechanical properties and fracture modes of SLM Ti–6Al–4V, Mater. Sci. Eng. A 616 (2014) 1–11, http://dx.doi.org/10.1016/j.msea.2014.07.086.

[35] H.L. Wei, J. Mazumder, T. DebRoy, Evolution of solidification texture during additive manufacturing, Sci. Rep. 5 (2015) 16446, http://dx.doi.org/10.1038/srep16446.

[36] S. Cai, M.R. Daymond, Y. Ren, Stress induced martensite transformation in Co–28Cr–6Mo alloy during room temperature deformation, Mater. Sci. Eng. A 580 (2013) 209–216, http://dx.doi.org/10.1016/j.msea.2013.05.050.

[37] EOS, Material data sheet EOS CobaltChrome MP1, Munique, 2011.

[38] S. Kurosu, H. Matsumoto, A. Chiba, Isothermal phase transformation in biomedical Co-29Cr-6Mo alloy without addition of carbon or nitrogen, Metall. Mater. Trans. A. 41 (2010) 2613–2625, http://dx.doi.org/10.1007/s11661-010-0273-8.

[39] A.D.J. Saldívar García, A.M. Medrano, A.S. Rodríguez, Formation of hcp martensite during the isothermal aging of an fcc Co-27Cr-5Mo-0.05C orthopedic implant alloy, Metall. Mater. Trans. A 30 (1999) 1177–1184, http://dx.doi.org/10.1007/s11661-999-0267-6.

[40] S. Kurosu, H. Matsumoto, A. Chiba, Grain refinement of biomedical Co-27Cr-5Mo-0.16N alloy by reverse transformation, Mater. Lett. 64 (2010) 49–52, http://dx.doi.org/10.1016/j.matlet.2009.10.001.

[41] K. Yamanaka, M. Mori, A. Chiba, Mechanical properties of as-forged Ni-free Co-29Cr-6Mo alloys with ultrafine-grained microstructure, Mater. Sci. Eng. A 528 (2011) 5961–5966, http://dx.doi.org/10.1016/j.msea.2011.04.027.

[42] C. Blochwitz, W. Tirschler, Twin boundaries as crack nucleation sites, Cryst. Res. Technol. 40 (2005) 32–41, http://dx.doi.org/10.1002/crat.200410305.

[43] Z.W. Wang, Y.B. Wang, X.Z. Liao, Y.H. Zhao, E.J. Lavernia, Y.T. Zhu, Z. Horita, T.G. Langdon, Influence of stacking fault energy on deformation mechanism and dislocation storage capacity in ultrafine-grained materials, Scr. Mater. 60 (2009) 52–55, http://dx.doi.org/10.1016/j.scriptamat.2008.08.032.

[44] C.J. Youngdahl, J.R. Weertman, R.C. Hugo, H.H. Kung, Deformation behavior in nanocrystalline copper, Acta Mater. 44 (2001) 1475–1478, http://dx.doi.org/10.1016/S1359-6462(01)00712-6.

[45] S. Kurosu, H. Matsumoto, A. Chiba, Isothermal phase transformation in biomedical Co-29Cr-6Mo alloy without addition of carbon or nitrogen, Metall. Mater. Trans. A 41 (2010) 2613–2625, http://dx.doi.org/10.1007/s11661-010-0273-8.

[46] R. Singh, R.D. Doherty, Strengthening in multiphase (MP35N) alloy: Part II, Elev. Temp. Tensile Creep Deform. 23 (1992) 321–334.

[47] Y. Chen, Y. Li, Y. Koizumi, H. Haider, A. Chiba, Effects of carbon addition on wear mechanisms of CoCrMo metal-on-metal hip joint bearings, Mater. Sci. Eng. C 76 (2017) 997–1004, http://dx.doi.org/10.1016/j.msec.2017.03.211.

[48] S. Lee, E. Takahashi, N. Nomura, A. Chiba, Effect of carbon addition on microstructure and mechanical properties of a wrought Co-Cr-Mo implant alloy, Mater. Trans. 47 (2006) 287–290, http://dx.doi.org/10.2320/matertrans.47.287.